Article:
AlAlaween, W.H., AlAlawin, A.H., AbuHamour, S.O. et al. (2023) Fuzzy particle swarm for the right-first-time of fused deposition. Journal of Intelligent & Fuzzy Systems, 45 (6). pp. 11977-11991. ISSN: 1064-1246

https://doi.org/10.3233/jifs-232135

Fuzzy Particle Swarm for the Right-First-Time of Fused Deposition

Wafa' H. AlAlaween[a*], Abdallah H. AlAlawin[b], Belal M.Y. Gharaibeh[a,c], Mahdi Mahfouf[d], Ahmad Alsoussi[e], Ashraf E. AbuKaraky[f] and Saif O. AbuHamour[f]

[a]*Department of Industrial Engineering, The University of Jordan, Amman, Jordan.*
[b] *Department of Industrial Engineering, Faculty of engineering, The Hashemite University, Zarqa, Jordan.*
[c] *Collage of Engineering and Applied Sciences, American University of Kuwait, Salmiya, Kuwait.*
[d]*Department of Automatic Control and Systems Engineering, The University of Sheffield, UK.*
[e]*Printie 3D Company, Amman, Jordan.*
[f]*Department of Oral and Maxillofacial Surgery, Oral Medicine and Periodontology, The University of Jordan, Amman, Jordan.*

Abstract. Right-first-time production enables manufacturing companies to be profitable as well as competitive. Ascertaining such a concept is not as straightforward as it may seem in many industries, including 3D printing. Therefore, in this research paper, a right-first-time framework based on the integration of fuzzy logic and multi-objective swarm optimization is proposed to reverse-engineer the radial based integrated network. Such a framework was elicited to represent the fused deposition modelling (FDM) process. Such a framework aims to identify the optimal FDM parameters that should be used to produce a 3D printed specimen with the desired mechanical characteristics right from the first time. The proposed right-first-time framework can determine the optimal set of the FDM parameters that should be used to 3D print parts with the required characteristics. It has been proven that the right-first-time model developed in this paper has the ability to identify the optimal set of parameters successfully with an average error percentage of 4.7%. Such a framework is validated in a real medical case by producing three different medical implants with the desired mechanical characteristics for a 21-year-old patient.

Keywords: Fuzzy logic, Particle swarm optimization, Radial based integrated network, Right-first-time production.

1. Introduction

Nowadays, additive manufacturing, as a key element of Industry 4.0, has been extensively employed in various areas such as medical, aerospace, manufacturing and tissue engineering [1]. This can be attributed to its ability to (i) produce complex and monolithic products with many features; and (ii) flexibly amend designs [2]. Although the working principles of the different additive manufacturing technologies are different, their essence of adding materials in a layer-upon-layer or surface-upon-surface fashion is, in general, the same [1]. The different additive manufacturing techniques consist of fused deposition modelling (FDM), resign-printing and laser sintering [3, 4]. Each technology has its own applications and strengths and limitations. Among them all, FDM is the most common technology employed in many applications [5]. Therefore, a huge body of research has focused on analyzing, modelling and optimizing this technology and the various thermoplastic polymers that can be printed [6].

Various papers have investigated the printability of various thermoplastic polymers (e.g., Polyether-ether-ketone (PEEK), Polyether-ketone-ketone (PEKK) and Polycaprolactone) and the features of the 3D printed products for biomedical applications [6]. For example, both Polylactic acid (PLA) and hydroxyapatite reinforced PLA were printed using FDM to produce scaffolds and to analyze their mechanical, biocompatibility and biodegradability properties [7]. To enhance the obtained properties of scaffolds without affecting

*Corresponding author. E-mail: w.alaween@ju.edu.jo.

the rheological properties, nanohydroxyapatite and polyvinyl alcohol were added to PLA to obtain a structure that is similar to bones [8, 9]. In addition, the PEEK material and the carbon-enhanced version were employed to print different orthopaedic and dental parts [10]. In addition to the various properties of the materials printed, the operation and the machine parameters have been examined [1, 11]. These parameters should be determined and optimized carefully in order to obtain the desired characteristics of the 3D printed products. Thus, many research papers have presented different experimental as well as statistical algorithms to define and optimize these parameters [12]. A comparative analysis was, for example, conducted to estimate the interrelationships among material- and machine-related parameters and the characteristics of the parts printed [13]. Likewise, the correlation analysis and the analysis of variance were utilized to statistically examine the effects of various parameters (e.g., orientation) on the characteristics of parts printed using different types of materials [14-18]. Furthermore, image correlation was employed to demonstrate the direct relationship between the material thickness and the characteristics of printed parts [19]. Likewise, several research studies have been previously devoted to systematically mapping the FDM variables to the features of the printed parts. For different materials, the artificial neural network was, for instance, developed to map various FDM parameters to the strength of the printed parts [20, 21]. In addition to improving the generalization abilities of the neural network, it was combined with the dimensional analysis conceptual modelling to enhance the understanding of the FDM process [22]. Moreover, a radial based integrated network was proposed to simulate the FDM process and to systematically and accurately anticipate the characteristics of 3D printed parts [5]. Likewise, fuzzy logic systems were utilized to simulate the FDM process and to extract a linguistic understanding [23].

The many research studies in the related literature have provided a good understanding of 3D printing, in particular the FDM process, and presented various statistical and intelligent models that can be utilized to anticipate the features of the printed specimens. However, to the best of our knowledge, none of these studies has investigated the utilization of a right-first-time structure to identify the optimal 3D printing parameters that need to be used to 3D print parts with required characteristics, this being due to the fact that inverting highly nonlinear and complex models may not be a straightforward task that leads to a unique set of FDM parameters. Therefore, in this research paper, the radial based integrated network that was presented in [5] is utilized in a right-first-time framework. Such a framework is proposed to identify the FDM parameters that should be used to 3D print specimens with the desired mechanical characteristics. In general, inverting highly nonlinear models usually leads to sets of parameters particularly when conflicting objectives need to be considered. Therefore, multi-objective optimization paradigms are commonly employed to identify a set of optimal solutions. Many multi-objective paradigms such as evolutionary and genetic ones have been implemented to find such a set of optimal solutions [24]. Because of its computational efficiency, a stochastic-based particle swarm optimization algorithm has been widely utilized [25, 26]. However, all multi-objective optimization algorithms including the particle swarm optimization cannot identify a single optimal solution. Many research papers have addressed this issue by presenting various methods [27]. However, there is no standard method that can be employed to provide the single/global optimal solution and replace the Pareto optimal set [28]. Therefore, the proposed right-first-time structure integrates the stochastic multi-objective particle swarm optimization and fuzzy logic in a way that can (i) effectively invert the radial based integrated network that was developed in [5]; and (ii) systematically identify the optimal set of the FDM parameters that need to be used to print 3D parts with the desired characteristics according to defined criteria. The right-first-time framework is then validated using a real medical case where three medical parts need to be produced with desired characteristics and then implanted in a 21-year-old patient. This paper is organized as follows: Section 2 discusses the experimental work. Section 3 proposes the right-first-time framework and presents the theoretical background of the radial based integrated network, and the integration of particle swarm optimization and fuzzy logic. The implementation and the results obtained are summarized in Section 4, whereas Section 5 presents the medical case and the validation of the proposed framework. Concluding remarks are finally discussed in Section 6.

2. Experimental work

High-performance polymers, namely, PEEK and PEKK (3DXTECH Additive Manufacturing, Grand Rapids Michigan, USA) were utilized to print ASTM-D638 specimens. A FUNMAT HT printer (INTAMSYS Technology Inc., Minneapolis, USA) was employed to print these specimens using different sets of FDM variables. The software used in this printer to

convert the design model to a GCODE format was InstamSuite 3.6.2. Eight FDM variables that can significantly determine the mechanical characteristics of the ASTM-D638 specimens and, thus, the properties of printed parts in general, are investigated in this paper. Such parameters with their levels are shown in Figure 1. These parameters were examined, in this research work, using partial factorial design of experiments designed according to the Taguchi L18 array. Therefore, 36 experiments were performed for PEEK and PEKK. To ensure measurement repeatability, each one of these experiments was repeated three times.

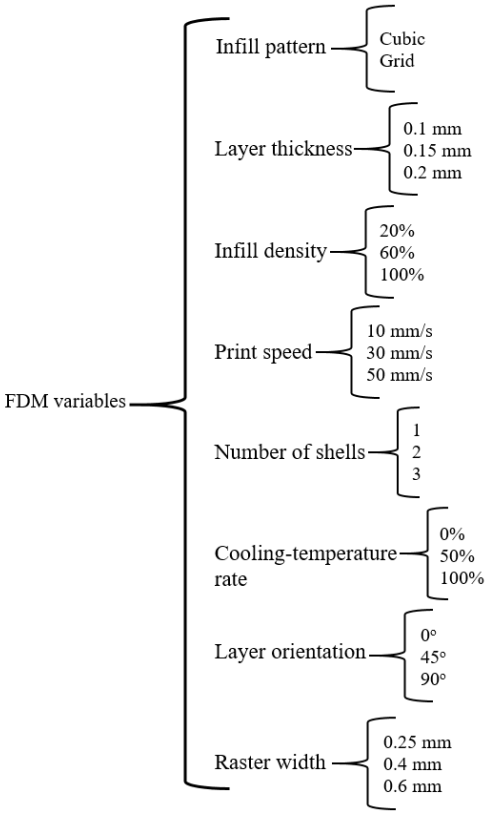

Figure 1 The fused deposition variables and their levels.

Once the printing of the standard specimens was completed, they were separated from the glass plate of the FUNMAT HT printer to cool down. Based on the manufacturer's recommendations, PEKK parts were annealed. All the printed specimens were then characterized in terms of their mechanical characteristics. Instron (SHIMADZU, USA) and the micro Vickers hardness tester (HTMV 2000M, echo LAB, Italy) were used to measure the ultimate tensile strength and elongation, and the micro-hardness, respectively. The average of the three measurements for each experiment was then determined. While measuring the strength and elongation, it was noted that the specimens' fracture was different in terms of the patterns and locations [5]. In addition, the mechanical behaviours of the printed specimens were different when compared to those of the original filaments. To elucidate, the ultimate tensile strength and the elongation values have decreased and increased, respectively, after 3D printing PEEK and PEKK. Furthermore, the FDM variables differently affected these characteristics of the specimens made using PEEK and PEKK. Figure 2 shows the correlation coefficients among the investigated parameters and the mechanical characteristics. In addition to the reasonable correlation values, such a figure shows that the relationships among them depend on the materials used. Furthermore, the print orientation has direct and strong inverse relationships with elongation for PEEK and PEKK, respectively. Also, the raster width, for instance, directly and inversely affected the tensile strength and elongation and micro-hardness, respectively. The speed has almost a negligible effect on micro-hardness for PEEK but a considerable one for PEKK. Since the infill pattern is considered to be a categorical variable, it was statistically analysed by employing the analysis of variance. It was noticed that it has considerable effects on all the mechanical characteristics of the two materials with p-values of less than 0.05.

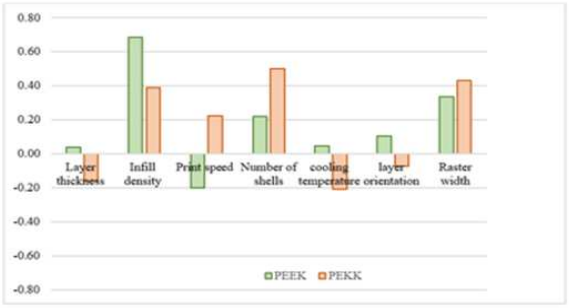

(a)

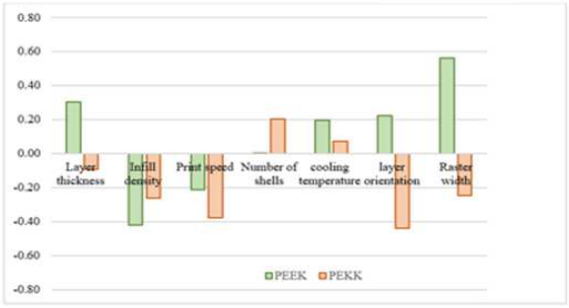

(b)

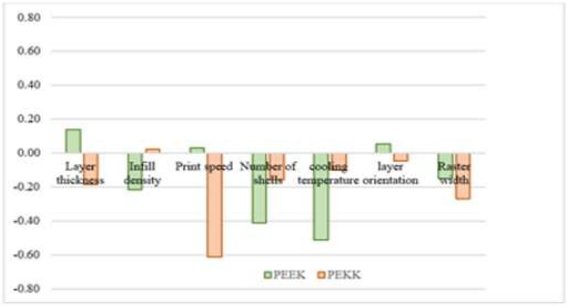

(c)

Figure 2 The correlation coefficients for (a) Strength; (b) Elongation; and (c) Micro-hardness.

3. The Right-First-Time Framework

Being able to develop cost-effective customized products, reducing waste, as well as enhancing supply chain and inventory management are features that companies in different industries strive to achieve. This can be attributed to their potential advantages that make companies profitable as well as successful. In addition, they allow them to gain leverage in today's highly competitive environment [29, 30]. Ascertaining such features systematically may not be as simple as it appears at the first glance, in particular, for those industries whose (i) processes are highly dimensional, and (ii) products affect customer health and well-being. One of these industries is additive manufacturing or the so-called 3D printing whose various processes, particularly the FDM process, are highly dimensional because of the many printing parameters that impact the quality attributes of 3D printed products. Likewise, the FDM process has been recently used to produce products in the medical and tissue engineering areas. Thus, the quality attributes of the products produced need to be as defined. In addition, the relationships among the printing parameters and their interactions and the quality attributes of these products are highly nonlinear. Therefore, this right-first-time structure is developed in this paper to deal with the aforementioned challenges and, thus, produce 3D printed parts with predefined quality characteristics right from the first time.

Figure 3 is a schematic diagram of the proposed right-first-time structure. Such a diagram consists of several stages. First, a set of experiments is conducted to collect the data required to build a data-driven model. The experimental work conducted in this research is briefly summarized in Section 2, where the effects of the eight parameters on the mechanical characteristics were examined. Second, a radial based integrated network, as a powerful data-driven model, was established to (i) represent the relationships between the printing parameters and the mechanical characteristics; and, thus, (ii) be used to predict these mechanical characteristics for any set of printing parameters that are within the investigated range. Finally, such a network was exploited in the reverse-engineering framework that is based on an optimization algorithm integrating PSO and fuzzy logic. Therefore, such a framework can identify the optimal set of the FDM printing parameters that need to be used to produce 3D printed parts with predefined mechanical characteristics. In other words, a 3D printed part with the predefined properties is produced right from the first time. It is worth mentioning that the presented structure is based on supervised algorithms, where the mechanical characteristics are required for the reverse-engineering framework. The radial based integrated network and the proposed optimization algorithm, which integrates PSO and fuzzy logic, are briefly presented in the following sub-sections to help readers in getting to grips with their theoretical backgrounds.

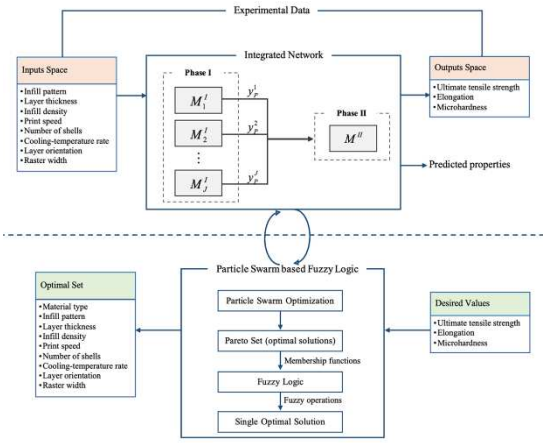

Figure 3 The newly proposed right-first-time framework for the FDM process.

3.1. Radial Based Integrated Network

Nowadays, data-based models have been used in various areas including, for example, pharmaceutics, manufacturing, diseases as well as automobiles [5, 30]. Such models, as the name indicates, and their predictive performances rely on the data utilized to develop them. To elucidate, the data used to develop data-driven models need to be representative in terms of, for example, their distribution and amount otherwise biased and inefficient models may result from unrepresentative data [29]. Acquiring such data is considered to be one of the challenging tasks in developing these models in particular, for the FDM process. This is because of the different FDM parameters that affect the features of the 3D parts, and their highly nonlinear interactions and relationships with the characteristics of these parts [1]. Thus, an integrated network based on radial basis functions is introduced to model such a process in two phases. In the first phase, a number of radial basis function (RBF) paradigms are utilized to simulate the FDM process by mapping its inputs to the mechanical characteristics. It is worth noting that these RBF networks may have different numbers of RBFs in the hidden layer and different values for their parameters. In the second phase, the outputs of these functions are mapped again to the mechanical characteristics leading to the predicted ones. Such two phases lead to a dense paradigm in a highly dimensional convex space and, as a result, it can (i) represent the possible relationships in the data available; (ii) improve the predictive performance; and (iii) deal with a limited number of sparse data points [5].

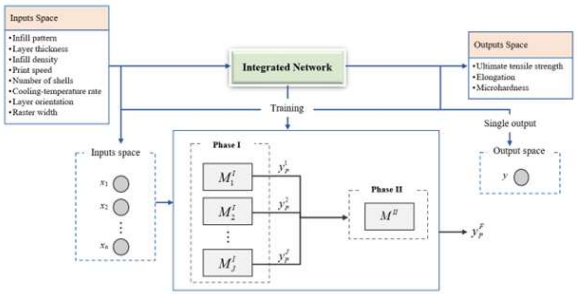

Figure 4 The schematic diagram of the integrated network [5].

The schematic representation of the radial basis integrated network is presented in Figure 4. First, the FDM parameters represented symbolically by the vector ($\mathbf{x}=x_1, x_2, \ldots, x_n$) are mapped using J RBF networks to each mechanical characteristic represented symbolically by the parameter y. Since these networks have different numbers of RBFs and different parameters, such a structure facilitates capturing and simulating all the possible relationships in the data provided. Once these models are successfully developed and their parameters are optimized, their outputs represented by the vector ($\mathbf{y_p}=y_{P1}, y_{P1}, \ldots, y_{P1}$) are then mapped by another RBF network to the output to lead to the final predicted one (y_p^F). Therefore, the mathematical representation of these two phases can be as follows [31]:

$$y_p^F(\mathbf{x}) = \sum_{j=1}^{J} \lambda_j^{(2)} \xi_j \left(\sum_{i=1}^{I} \lambda_i^{(1)} \xi_i(\mathbf{x}) + \lambda_o^{(1)} \right) + \lambda_o^{(2)} \qquad (1)$$

where ξ_i, λ_i and λ_o stand for the i^{th} RBF and its weight and bias, respectively. The superscript (1) and (2) are used to distinguish the weights and bias used in the first phase from those used in the second one, respectively. Such a mathematical representation presents y_p^F as composition and superposition of the RBFs. This makes the function dense in the space and, thus, improves the predictive performance [5]. The RBF shown in Eq.(1) plays a significant role in the performance of the integrated network. Various types of such a function can be employed such as polyharmonic spline and bump functions [32]. In this research work, the Gaussian function is employed. Such a function is commonly presented as follows [5]:

$$\xi_i(\mathbf{x}) = \exp\left(-\frac{(x-\mu_i)^2}{2\sigma_i^2} \right) \qquad (2)$$

where μ_i and σ_i symbolize the mean and standard deviation, respectively. In addition to the weight and bias

presented in Eq. (1), the mean and standard deviation values are commonly initialized randomly and, then, their optimal values are usually determined by an optimization algorithm embedded in the backpropagation network. In this research work, the scaled conjugate gradient (SCG) algorithm was employed.

3.2. Particle Swarm based Fuzzy Logic Optimization

Nature-inspired optimization paradigms that include, for instance, genetic and evolutionary algorithms have hitherto received a lot of interest. Such paradigms have been presented to deal with nonlinear, continuous/discrete and multimodal optimization problems [27]. Among them all, PSO algorithms, as computational ones that imitate the motion of fishes and birds, can be considered to be the most common ones. This can be attributed to their effectiveness in estimating a global optimum and their computational efficiency in terms of fast convergence [33]. In general, PSO problems can be divided into single and multi-objective optimization problems. Many PSO paradigms have been utilized to deal with single objective problems. The good results obtained have led to extending them to solve multi-objective optimization problems [33]. In contrast to single objective optimization, solving multi-objective ones leads, in general, to a set of optimal solutions known as Pareto optimal, non-inferior or non-dominated set. Defining a single optimal solution from such a set has been an active research topic. Although many paradigms including, for instance, weighted sum and ranking approaches, have been proposed, defining a single optimal solution remains an attractive research topic [24]. Therefore, a new optimization paradigm based on embedding fuzzy logic in the PSO model is presented to solve multi-objective optimization problems. This can be attributed to the fact that fuzzy logic can handle uncertainties in a natural and efficient way [24].

In general, unconstrained multi-objective optimization can be expressed as follows [34]:

$$\underset{x\in\Omega}{Min}\ F(x)=\left(f_1(x),f_2(x),\ldots f_N(x)\right) \qquad (3)$$

where **x** stands for an n-dimensional vector of decision variables defined in the decision space ($\boldsymbol{\Omega}$). In real-life cases, the values of the decision vector are subject to a number of equality and inequality constraints. This leads to a constrained multi-objective optimization model [34]. In order to find the Pareto set of optimal solutions using a PSO algorithm, a set of particles representing possible values of the decision variables (i.e., potential solutions) are initialized randomly in the search space, the so-called feasible space. Such particles are commonly described by their positions ($\mathbf{x}^i = x_{i1}, x_{i2}, \ldots, x_{in}$) as well as their velocities ($\mathbf{v}^i = v_{i1}, v_{i2}, \ldots, v_{in}$). Based on the particles' experience, the particles' positions and velocities are revised during the search. Depending on their values at the t^{th} iteration, the position and velocity of the i^{th} particle for the next iteration (t+1) can therefore be determined as follows [35]:

$$\begin{aligned} v_{ij}^{t+1} &= v_{ij}^{t} + c_1 r_1\left(p_{ij}^{t} - x_{ij}^{t}\right) + c_2 r_2\left(p_{gj}^{t} - x_{ij}^{t}\right) \\ x_{ij}^{t+1} &= x_{ij}^{t} + v_{ij}^{t+1} \end{aligned} \qquad (4)$$

where r_1 and r_2 stand for random numbers in the range from 0 to 1. In addition, c_1 and c_2 stand for the learning factors reflecting the impact of the local and the global optima, respectively. It is worth emphasising that the learning factors can be kept fixed or dynamically changed during the optimization process [24]. In this research work, and for simplicity and due to the intensity of the integrated network calculations, the learning factors were kept constant at a value of 2. In order to keep the particles in the feasible solutions space, the velocities need to be in the predefined range of $v_{\min}$ to $v_{\max}$. These equations are applicable for continuous decision variables. For the discrete variables, the velocity needs to be converted to a probability vector (τ_{ij}^{t}) using commonly the sigmoid function as follows [35]:

$$\tau_{ij}^{t} = \frac{1}{1+e^{-v_{ij}^{t+1}}} \qquad (5)$$

the t+1 position is one if a random number is less than such a probability vector, and it is zero if the random number is greater than or equal to such a vector [35]. Once the set of Pareto optimal solutions is found, a single one can be identified using fuzzy logic. According to predefined criteria, a set of clusters can be identified in the space. It is worth mentioning that many criteria can be utilized and there is no need for the number of criteria and the number of objective functions to be equal. For a right-first-time framework, the predictive performance can be considered as a criterion that can determine the set of the process parameters that need to be used to obtain a set of predefined characteristics, and can make sure that a good predictive performance is achieved. Such a step is followed

by estimating the membership value (μ_i) for the i^{th} solution in the optimal set. The membership value can be determined using the Gaussian membership function as follows [36]:

$$\mu_i = \exp\left(\frac{-(P_{x_i} - M)^2}{2\times\sigma^2}\right) \quad (6)$$

where P_{x_i}, M and σ represent the performance of the i^{th} solution, mean and the standard deviation of each cluster, respectively. Once such values are determined for the predefined criteria, they are integrated for each defined solution by the well-known fuzzy operations that include, but not limited to, minimum and product. Such operations need to be used according to the optimization problem investigated and the criteria identified.

4. Model Implementation and Results

The radial based integrated network, which briefly summarized in Section 3.1, was employed in a reverse-engineering structure to allow the right-first-time manufacturing of 3D printed parts with the required mechanical characteristics using the optimization algorithm presented in this paper. First and based on the experimental data, the radial based integrated networks with 10 RBF networks and an RBF network in the first and second phases, respectively, were developed to map the printing parameters summarized in Figure 1 to the three mechanical characteristics investigated, and, then, to predict these characteristics. The performance obtained for the tensile strength, as an example, is shown in Figure 5. In addition, the coefficient of determination (R^2), the root mean square error (RMSE), the mean absolute percentage error (MAPE), scatter index and bias for all the networks are summarized in Table 1, which shows good predictive performances for all the mechanical characteristics. For comparison purposes, the RBF model, the artificial neural network (ANN) and fuzzy logic system (FLS) were also developed to the map the 3D printing to the three mechanical characteristics. For the ultimate tensile strength, the overall performance measures in terms of [R^2, RMSE] for the RBF, ANN and FLS are [0.82, 8.83], [0.78, 10.91] and [0.80, 9.49], respectively. For elongation, the overall performance measures in terms of [R^2, RMSE] for the RBF, ANN and FLS are [0.73, 5.48], [0.69, 6.4] and [0.74, 5.8], respectively. For micro-hardness, the overall performance measures in terms of [R^2, RMSE] for the RBF, ANN and FLS are [0.68, 2.83], [0.68, 2.84] and [0.71, 2.78], respectively. These performance measures for the different models show that the radial based integrated network outperformed these well-known data-based models.

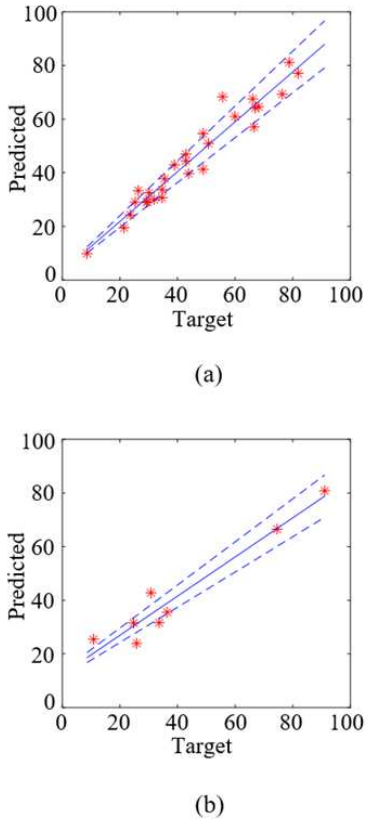

Figure 5 The radial based integrated network performance for the strength with a 90% band [5].

Table 1 The performance measures for the integrated networks.

Performance measures		Output		
		Ultimate tensile strength	Elongation	Micro-hardness
R^2	Training set	0.94	0.93	0.90
	Testing set	0.91	0.91	0.91
RMSE	Training set	5.40	2.30	1.30
	Testing set	5.90	7.60	1.40
MAPE	Training set	0.19	0.13	0.06
	Testing set	0.20	0.15	0.06
Scatter index	Training set	0.20	0.19	0.81
	Testing set	0.20	0.21	0.83
Bias	Training set	-0.05	0.001	0.06
	Testing set	-0.08	0.001	-0.013

Since three mechanical properties were investigated, a multi-objective PSO optimization model was employed. Therefore, the optimization mathematical model can be expressed as follows:

$$\text{Minimize} \quad \left\{ J^S = \left| \frac{\gamma_P^S}{\gamma_D^S} - 1 \right|, \quad J^E = \left| \frac{\gamma_P^E}{\gamma_D^E} - 1 \right|, \quad J^M = \left| \frac{\gamma_P^M}{\gamma_D^M} - 1 \right| \right\}$$

Subject to:

$$\begin{aligned} & x_j^{\min} \le x_j \le x_j^{\max} \qquad j = 3,4,...,9 \\ & x_1 = \begin{cases} 0 & \text{if PEEK material is used} \\ 1 & \text{if PEKK material is used} \end{cases} \\ & x_2 = \begin{cases} 0 & \text{if Cubic pattern is used} \\ 1 & \text{if Grid pattern is used} \end{cases} \end{aligned} \tag{7}$$

where γ_P and γ_D represent the predicted and the desired values of the mechanical characteristics, the superscripts S, E and M stand for strength, elongation and micro-hardness. The parameter x_j stands for the j^{th} parameter of the position vector of the i^{th} solution. The continuous set of constraints guarantees that the continuous FDM parameters are within the examined ranges as presented in [5], whereas the discrete ones ensure that specific types of materials and patterns are used. Based on the experimental work, the mathematical model in (7), that needs to be used to produce 3D parts with an ultimate tensile strength value of 100MPa, an elongation value of 22% and a micro-hardness value of 30 can be expressed as follows:

$$\text{Minimize} \quad \left\{ J^S = \left| \frac{\gamma_P^S}{100} - 1 \right|, \quad J^E = \left| \frac{\gamma_P^E}{22} - 1 \right|, \quad J^M = \left| \frac{\gamma_P^M}{30} - 1 \right| \right\}$$

Subject to:

$$\begin{aligned} & x_1 = \begin{cases} 0 & \text{if PEEK material is used} \\ 1 & \text{if PEKK material is used} \end{cases} \\ & x_2 = \begin{cases} 0 & \text{if Cubic pattern is used} \\ 1 & \text{if Grid pattern is used} \end{cases} \\ & 0.1 \le x_3 \le 0.2 \\ & 20 \le x_4 \le 100 \\ & 10 \le x_5 \le 50 \\ & 1 \le x_6 \le 3 \\ & 0 \le x_7 \le 1 \\ & 0 \le x_8 \le 90 \\ & 0.25 \le x_9 \le 0.6 \end{aligned} \tag{8}$$

Such a mathematical model was solved using the algorithm presented in Section 3.2, where multi-objective PSO was first used to identify the Pareto optimal set by randomly initializing 300 particles for 300 iterations. Figures 6-8 show some examples of the behaviours of these three objectives in the search area. It is apparent that these three objectives are in conflict. To illustrate, improving one of them may deteriorate the other objectives. For example, increasing the print speed and decreasing the infill density decrease the strength objective but increase the elongation and the micro-hardness objectives. It is also apparent that the behaviors of the objectives are not as continuous as it was expected. This can be attributed to the effect of the two discrete variables, namely, the type of materials and the infill pattern, on these three objectives.

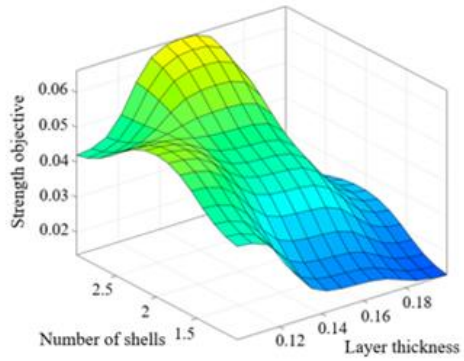

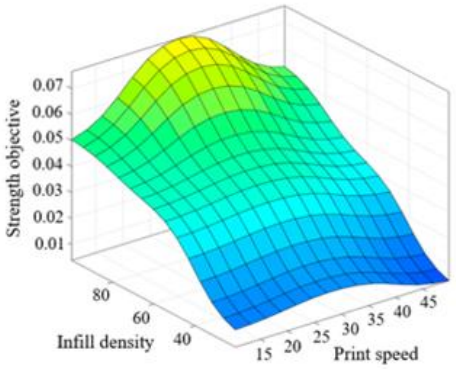

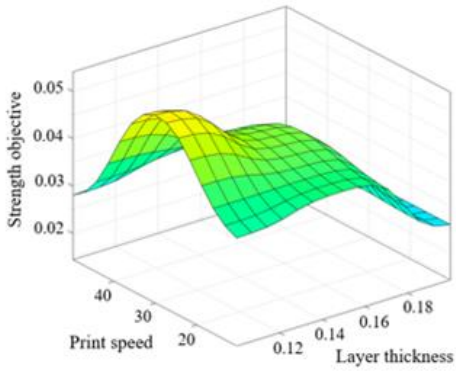

Figure 6 Examples of the 3D surfaces for the ultimate tensile strength objective.

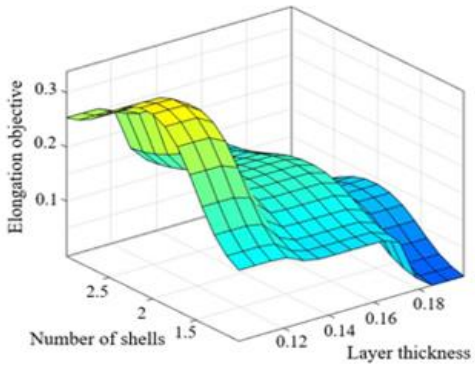

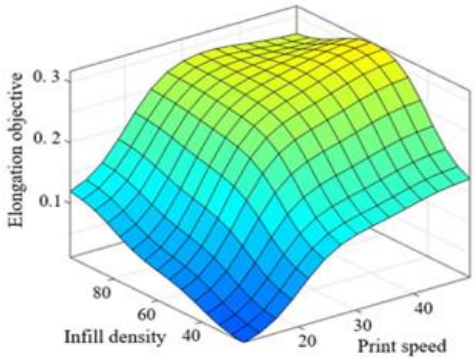

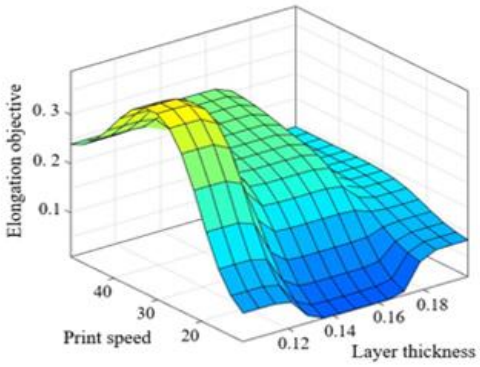

Figure 7 Examples of the 3D surfaces for the elongation objective.

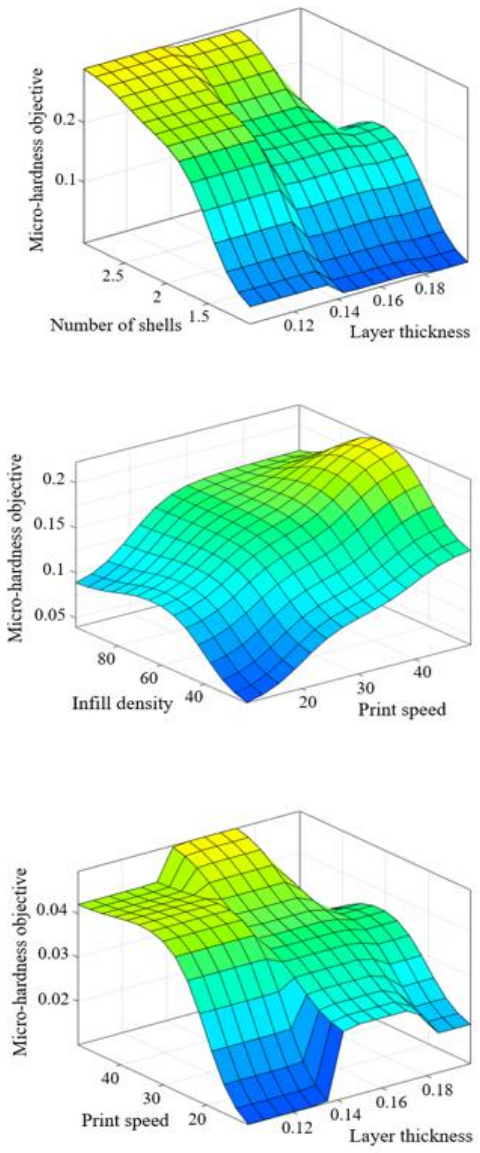

Figure 8 Examples of the 3D surfaces for the micro-hardness objective.

The number of optimal solutions in the Pareto optimal set is relatively large. Therefore, Figure 9 presents the Pareto set that was obtained by solving the model presented in Eq. (8).

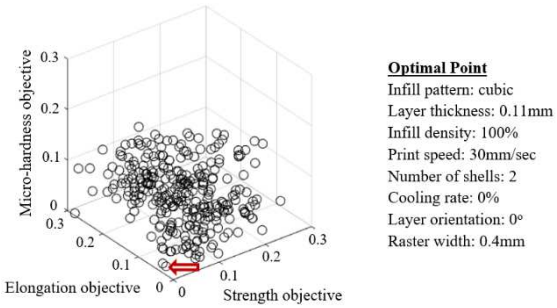

Figure 9 The Pareto solutions defined by the multi-objective PSO algorithm (the optimal solution obtained by fuzzy logic is highlighted by the red arrow).

Once such a set was identified, the optimum point can be selected. Many criteria can be used to define such a point depending on the preferences and priorities of users. For the right-first-time model, the performance of the radial based integrated network in the area examined was considered to be the main criterion in selecting the single optimal solution. Therefore, the FDM printing parameters and the error values resulting from the network were employed to identify the network's performance in the space. Such a performance can be grouped into three clusters, namely, Unsatisfactory, Satisfactory and Excellent. For the strength, the performance of the radial based network in one of the space areas, as an example, is shown in Figure 10. Such a figure states that the performance of the radial based integrated network is satisfactory when the material is PEEK, infill pattern is grid, layer thickness is low, infill density is low, print speed is high, number of shells is high, cooling rate is low, layer orientation is medium and raster width is low.

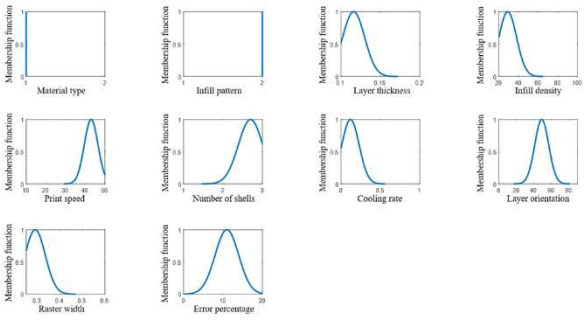

Figure 10 An example of the performance of the integrated model in one of the space areas.

For the Pareto optimal solutions identified in Figure 9,

the membership values were determined using Eq. 6. It is worth mentioning that each solution has three membership values for each cluster for the three mechanical characteristics. Such membership values can be integrated by employing various fuzzy operations. In this research work, the product operation was used. The solution of the Pareto set that has the maximum membership value was chosen to be the single optimal solution. Therefore, the FDM parameters that need to be used to produce 3D printed specimen with an ultimate tensile strength value of 100MPa, an elongation value of 22% and a micro-hardness value of 30 are presented in Figure 9 for PEEK. This optimal point is marked by the arrow in Figure 9, where it is apparent that slight changes in these values may deteriorate at least one of the three objectives. The FDM parameters for such a point are listed in Figure 9. Three standard specimens were printed using the optimal set of parameters identified (or close value to them). The values of the ultimate tensile strength, elongation and microhardness of these specimens were experimentally measured. The average values of the ultimate tensile strength, elongation and microhardness are 95.4MPa, 22.9 and 28.3, respectively. It is noticeable that the right-first-time model developed in this paper has the ability to identify the optimal set of parameters successfully with an average error percentage of 4.7%.

5. Right-First-Time Validation: Medical Implants

Following Research Ethics Board approval and in order to validate the right-first-time framework proposed in this research work, three medical implants for a 21-year-old patient suffering from Hemifacial Microsomia, as shown in Figure 11, were produced using 3D printing. Clinical examination revealed an underdeveloped left side of the face and malformation of the left ear lobe without hearing problems. The zygomatic bone and the ramus of the mandible on the ipsilateral side were smaller in size compared to the ones on the right side. In addition, he has weak left-side facial muscles. It is worth mentioning that a mandibular distraction osteogenesis surgery was performed for the patient a year ago leading to an incomplete correction of facial asymmetry. Therefore, implants are required in such a case. A CBCT x-ray was taken for the patient and represented in the Digital Imaging and Communications in Medicine (DICOM) format. Various 3D design programs, namely, Meshmixer®, Slicer® and Blender® were then employed to design patient-specific implants by mirroring the non-affected side. Such implants were printed by the FUNMAT HT 3D printer using PEEK, as a biocompatible material. The surgeons at The University of Jordan Hospital defined the values of the mechanical characteristics of the implants (i.e., the ultimate tensile strength value of 105MPa, an elongation value of 20% and a microhardness value of 30).

The optimal set: cubic infill pattern, a layer thickness of 0.156mm, an infill density of 94%, a print speed of 28mm/s, a number of shells of 3, a cooling-temperature rate of 0%, a layer orientation of 3° and a raster width of 0.42mm.

Figure 11 The patient scans and the two implants produced using the optimal set.

The right-first-time structure was utilized to identify the FDM parameters that need to be used to print the implants to obtain the required values of the mechanical characteristics. Therefore, the framework was implemented as described in Section 4. The optimal set of the FDM parameters is summarized in Figure 11. By using these parameters (or close value to them), the implants were produced using PEEK. The three parts implants are shown in Figure 12. It is worth noting that medical-grade PEEK was printed to produce these implants. Since these implants need to be attached to the zygomatic and ramus of mandible bones by Titanium screws, screw holes were predrilled in the implants at different locations as recommended by the surgeons. Such a step was followed by sterilizing the implants using autoclaving technique. Such sterilized implants were then implanted in the patients during a 4-hour operation, in which the patient was under general anesthetic. Figure 13 shows the implants attached to the zygomatic and ramus of mandible bones during the surgery.

Figure 12 The three customized implants printed for the patient.

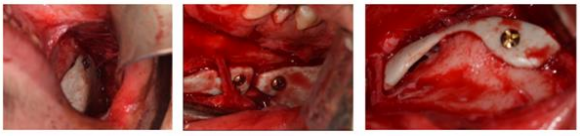

Figure 13 The implants attached to the zygomatic and ramus of mandible bones.

6. Conclusion

A right-first-time structure based on the integration of fuzzy logic and multi-objective particle swarm optimization was proposed to reverse-engineer the radial based integrated network developed to represent fused deposition modelling (FDM). The proposed structure was successful in identifying the optimal set of the FDM parameters that need to be used to produce 3D printed parts with predefined values of the mechanical characteristics. It was noticeable that the radial based integrated network developed to represent the FDM process outperformed three well-known models (i.e., The radial based function, the artificial neural network and the fuzzy logic system). Likewise, the right-first-time model developed in this paper was able to identify the optimal set of parameters successfully with an average error percentage of 4.7%. The proposed framework was validated by printing 3D medical implants for a 21-year-old patient suffering from Hemifacial Microsomia. In summary, the proposed framework is truly promising in the additive manufacturing industry, and, as a result, it can have several advantages in terms of meeting the stringent regulations in some of its applications, producing cost-effective customized implants/products, and minimizing time-to-market.

References

[1] C. Parulski, O. Jennotte, A. Lechanteur, and B. Evrard, "Challenges of fused deposition modeling 3D printing in pharmaceutical applications: Where are we now?," *Advanced Drug Delivery Reviews,* vol. 175, p. 113810, 2021.

[2] W. H. AlAlaween *et al.*, "A dynamic nonlinear autoregressive exogenous model for the prediction of COVID-19 cases in Jordan," *Cogent Engineering,* vol. 9, no. 1, p. 2047317, 2022.

[3] S. S. Crump, "Apparatus and method for creating three-dimensional objects," ed: Google Patents, 1992.

[4] E. M. Sachs, J. S. Haggerty, M. J. Cima, and P. A. Williams, "Three-dimensional printing techniques," ed: Google Patents, 1993.

[5] W. AlAlaween *et al.*, "The development of a radial based integrated network for the modelling of 3D fused deposition," *Rapid Prototyping Journal,* vol. ahead-of-print, no. ahead-of-print, 2022, doi: 10.1108/RPJ-04-2022-0121.

[6] D. Singh, A. Babbar, V. Jain, D. Gupta, S. Saxena, and V. Dwibedi, "Synthesis, characterization, and bioactivity investigation of biomimetic biodegradable PLA scaffold fabricated by fused filament fabrication process," *Journal of the Brazilian Society of Mechanical Sciences and Engineering,* vol. 41, no. 3, pp. 1-13, 2019.

[7] S. Singh, C. Prakash, and S. Ramakrishna, "3D printing of polyether-ether-ketone for biomedical applications," *European Polymer Journal,* vol. 114, pp. 234-248, 2019.

[8] C. Esposito Corcione, F. Gervaso, F. Scalera, F. Montagna, A. Sannino, and A. Maffezzoli, "The feasibility of printing polylactic acid–nanohydroxyapatite composites using a low-cost fused deposition modeling 3D printer," *Journal of Applied Polymer Science,* vol. 134, no. 13, 2017.

[9] M. Alizadeh-Osgouei, Y. Li, A. Vahid, A. Ataee, and C. Wen, "High strength porous PLA gyroid scaffolds manufactured via fused deposition modeling for tissue-engineering applications," *Smart Materials in Medicine,* vol. 2, pp. 15-25, 2021.

[10] A. Haleem, M. Javaid, A. Vaish, and R. Vaishya, "Three-dimensional-printed polyether ether ketone implants for orthopedics," *Indian Journal of Orthopaedics,* vol. 53, no. 2, p. 377, 2019.

[11] J. M. Nasereddin, N. Wellner, M. Alhijjaj, P. Belton, and S. Qi, "Development of a simple mechanical screening method for predicting the feedability of a pharmaceutical FDM 3D printing filament," *Pharmaceutical research,* vol. 35, no. 8, pp. 1-13, 2018.

[12] A. J. Sheoran and H. Kumar, "Fused Deposition modeling process parameters optimization and effect on mechanical properties and part quality: Review and reflection on present research," *Materials Today: Proceedings,* vol. 21, pp. 1659-1672, 2020.

[13] S. Khan, K. Joshi, and S. Deshmukh, "A comprehensive review on effect of printing parameters on mechanical properties of FDM printed parts," *Materials Today: Proceedings,* 2021.

[14] J. Chacón, M. A. Caminero, E. García-Plaza, and P. J. Núnez, "Additive manufacturing of PLA structures using fused deposition modelling: Effect of process parameters on mechanical properties and their optimal selection," *Materials & Design,* vol. 124, pp. 143-157, 2017.

[15] M. Ouhsti, B. El Haddadi, and S. Belhouideg, "Effect of printing parameters on the mechanical properties of parts fabricated with open-source 3D printers in PLA by fused deposition modeling," *Mechanics and Mechanical Engineering,* vol. 22, no. 4, pp. 895-907, 2018.

[16] A. A. Ansari and M. Kamil, "Effect of print speed and extrusion temperature on properties of 3D printed PLA using fused deposition modeling process," *Materials Today: Proceedings,* vol. 45, pp. 5462-5468, 2021.

[17] E. Carlier *et al.*, "Investigation of the parameters used in fused deposition modeling of poly (lactic acid) to optimize 3D printing sessions," *International Journal of Pharmaceutics,* vol. 565, pp. 367-377, 2019.

[18] A. Pandzic, D. Hodzic, and A. Milovanovic, "EFFECT OF INFILL TYPE AND DENSITY ON TENSILE PROPERTIES OF PLAMATERIAL FOR FDM PROCESS," *Annals of DAAAM & Proceedings,* vol. 30, 2019.

[19] Z. Xu, R. Fostervold, and S. M. J. Razavi, "Thickness effect on the mechanical behavior of PLA specimens fabricated via Fused Deposition Modeling," *Procedia Structural Integrity,* vol. 33, pp. 571-577, 2021.

[20] D. Yadav, D. Chhabra, R. K. Garg, A. Ahlawat, and A. Phogat, "Optimization of FDM 3D printing process parameters for multi-material using artificial neural network," *Materials Today: Proceedings,* vol. 21, pp. 1583-1591, 2020.

[21] J. Giri, P. Shahane, S. Jachak, R. Chadge, and P. Giri, "Optimization of FDM process parameters for dual extruder 3d printer using Artificial Neural network," *Materials Today: Proceedings,* vol. 43, pp. 3242-3249, 2021.

[22] H. P. Nagarajan *et al.*, "Knowledge-based design of artificial neural network topology for additive manufacturing process modeling: a new approach and case study for fused deposition modeling," *Journal of Mechanical Design,* vol. 141, no. 2, p. 021705, 2019.

[23] A. Trivedi and P. K. Gurrala, "Fuzzy logic based expert system for prediction of tensile strength in Fused Filament Fabrication (FFF) process," *Materials Today: Proceedings,* vol. 44, pp. 1344-1349, 2021.

[24] W. H. AlAlaween, A. H. AlAlawin, L. Al-Durgham, and N. T. Albashabsheh, "A new integrated modelling architecture based on the concept of the fuzzy logic for the turning process," *Journal of Intelligent & Fuzzy Systems,* no. Preprint, pp. 1-13, 2021.

[25] C. Qi, Q. Chen, X. Dong, Q. Zhang, and Z. M. Yaseen, "Pressure drops of fresh cemented paste backfills through coupled test loop experiments and machine learning techniques," *Powder Technology,* vol. 361, pp. 748-758, 2020.

[26] E. H. Houssein, M. E. Hosney, D. Oliva, W. M. Mohamed, and M. Hassaballah, "A novel hybrid Harris hawks optimization and support vector machines for drug design and discovery," *Computers & Chemical Engineering,* vol. 133, p. 106656, 2020.

[27] T. T. Vu, H. H. Kha, T. Q. Duong, and N.-S. Vo, "Particle swarm optimization for weighted sum rate maximization in MIMO broadcast channels," *Wireless Personal*

Communications, vol. 96, no. 3, pp. 3907-3921, 2017.

[28] W. H. Alalaween, A. H. Alalawin, M. Mahfouf, and O. H. Abdallah, "A Dynamic Type-1 Fuzzy Logic System for the Development of a New Warehouse Assessment Scheme," *IEEE Access,* vol. 9, pp. 43611-43619, 2021.

[29] A. H. AlAlawin, W. H. Alalaween, M. A. Salem, M. Mahfouf, N. T. Albashabsheh, and C. He, "A fuzzy logic based assessment algorithm for developing a warehouse assessment scheme," *Computers & Industrial Engineering,* vol. 168, p. 108088, 2022.

[30] W. H. AlAlaween, M. Mahfouf, and A. D. Salman, "When swarm meets fuzzy logic: Batch optimisation for the production of pharmaceuticals," *Powder Technology,* vol. 379, pp. 174-183, 2021.

[31] W. H. AlAlaween, M. Mahfouf, and A. D. Salman, "Integrating the physics with data analytics for the hybrid modeling of the granulation process," *AIChE Journal,* vol. 63, no. 11, pp. 4761-4773, 2017.

[32] C. M. Bishop and N. M. Nasrabadi, *Pattern recognition and machine learning* (no. 4). Springer, 2006.

[33] P. Shanmugavadivu and K. Balasubramanian, "Particle swarm optimized multi-objective histogram equalization for image enhancement," *Optics & laser technology,* vol. 57, pp. 243-251, 2014.

[34] R. C. Eberhart, Y. Shi, and J. Kennedy, *Swarm intelligence*. Elsevier, 2001.

[35] D. Wang, D. Tan, and L. Liu, "Particle swarm optimization algorithm: an overview," *Soft computing,* vol. 22, no. 2, pp. 387-408, 2018.

[36] J. M. Mendel, *Uncertain rule-based fuzzy logic systems: Introduction and new directions*. Prentice Hall, 2001.